

Tribocorrosion Behavior of Several Corrosion-resistant Alloys Sliding Against CF-PEEK: Application for Hydraulic Valve in Seawater

Fanglong Yin¹, Xin Zhou¹, Songlin Nie^{1,*}, Hui Ji¹ and Zhen Hu²

¹ Beijing Key Laboratory of Advanced Manufacturing Technology, Beijing University of Technology, Beijing 100124, China

² Department of Industrial and Manufacturing Systems Engineering, University of Michigan-Dearborn, Dearborn, MI 48128, USA

*E-mail: niesonglin@bjut.edu.cn

Received: 22 October 2018 / Accepted: 22 December 2018 / Published: 10 April 2019

To select appropriate combinations of antifriction and wear-resistant materials for key tribopairs in seawater hydraulic valves, the tribocorrosion behavior of six kinds of corrosion-resistant alloys sliding against a carbon fiber/polytetrafluoroethylene/graphite (CF/PTFE/graphite)-filled polyetheretherketone (CF-PEEK) composite under artificial seawater lubrication was comparatively investigated by using a pin-on-disk friction tester and electrochemical workstation. The results show that AISI 316, AISI 630 and chromium-plated Ti6Al4V exhibit better tribological behavior than Ti6Al4V and nitrided Ti6Al4V under dry friction, distilled water and artificial seawater conditions. Besides, Ti6Al4V exhibits better corrosion resistance than other corrosion-resistant alloys in both static corrosion and tribocorrosion conditions, and the chromium plating process significantly accelerates the Ti6Al4V corrosion rate in seawater. Moreover, the corrosion-induced wear is higher than the wear-induced corrosion. In addition, the contribution of corrosion-induced wear to synergetic weight loss is more than 85% for all the alloys under tribocorrosion in seawater. Consequently, material combinations of AISI 630/CF-PEEK and AISI 316/CF-PEEK could preferentially be used in seawater hydraulic valves.

Keywords: corrosion-resistant alloys, CF-PEEK, friction and wear, seawater hydraulic valves, tribocorrosion

1. INTRODUCTION

Seawater hydraulic transmission has inherent advantages when applied in ocean development equipment because of its environmental friendliness, seawater pressure self-compensation, low operating cost, easy disposal of working media, simplicity of system composition and cleanliness [1-3]. Seawater hydraulic valve is a critical control element of seawater hydraulic systems. Due to the low

viscosity, poor lubrication and strong corrosiveness of seawater, there are some technical problems, such as internal leakage and tribocorrosion wear failure, in the development of seawater hydraulic valves [4, 5]. As a result, the tribocorrosion properties of key tribopairs in seawater hydraulic valves are crucial to guarantee the performance and reliability of the valves. Therefore, the selection of appropriate material combinations that can improve the tribological and anticorrosive performance of the key tribopairs in seawater hydraulic valves, especially the spool-valve/seat pair, is a rather difficult problem.

Fortunately, the combination of engineering plastics and corrosion-resistant alloys has been reported as appropriate for the spool-valve/seat tribopair in seawater hydraulic valves [6, 7], and significant efforts have been reported regarding the tribological behavior of such combinations. The tribological characteristics of polytetrafluoroethylene (PTFE) sliding with GCr15 steel under air, distilled water, seawater and NaCl solution lubrication were comparatively studied [8]. It was concluded that the deposition of CaCO_3 and $\text{Mg}(\text{OH})_2$ layers could significantly reduce the wear rate and friction coefficients of the tribopair can be obtained in seawater because of the deposition of CaCO_3 and $\text{Mg}(\text{OH})_2$ layers. Among various engineering plastics, polyetheretherketone (PEEK) has excellent wear-resistance and tribological characteristics in water. Therefore, the tribological performance of PEEK sliding on AISI 630 stainless steel has been comprehensively investigated [9-12]. It was found that the carbon fiber (CF)-PEEK/AISI 630 stainless steel tribopair has good tribological performance in seawater.

Several attempts have been made to reveal the tribocorrosion behavior of corrosion-resistant alloys in seawater [13]. Chen [14] researched the tribocorrosion performance of Monel K500 and Ti6Al4V alloys sliding with AISI 316 stainless steel lubricated with water, and found that the friction coefficients were smaller under seawater lubrication than distilled water lubrication and that mechanical wear could damage the passive film and accelerate the corrosion rate. In addition, the static corrosion and tribocorrosion characteristics of AISI 316, Ti6Al4V and Monel K500 sliding on Al_2O_3 lubricated with artificial seawater has been investigated [15, 16]. It was concluded that the alloy wear loss was significantly increased by corrosion and that AISI 316 was less resistant to sliding damage than Ti6Al4V alloy. Zhang [17] investigated the tribocorrosion performance of the alumina/S31254 steel tribopair lubricated with seawater by using a triboelectrochemical technique and demonstrated that the positive synergy between wear and corrosion increased with the increase of applied potential lubricated with seawater.

In addition, there are some reports on the tribocorrosion performance of stainless steel with hardmetal coating lubricated with seawater. Shan [18] investigated the tribocorrosion performance of AISI 316L and AISI 316L with CrN coating sliding against Si_3N_4 lubricated with seawater. The static corrosion and the contribution of wear-induced corrosion increased with increasing potential. Zhou [19] researched the tribological properties of 316L stainless steel with different CrN-based coatings and found that the tribocorrosion performance of CrBCN coatings was better than that of CrCN coatings.

Although many researches has been conducted to investigate the tribological behavior of engineering plastics and stainless steel and the tribocorrosion behavior of corrosion-resistant alloys and hardmetal-coated stainless steel in seawater, the tribocorrosion behavior of corrosion-resistant alloys sliding against PEEK under seawater lubrication is still uncertain and remains to be further studied. It

has been reported that tribopairs consisting of corrosion-resistant alloys and PEEK may be appropriately used in seawater hydraulic components. In addition, it has been found that PEEK contained 30 vol.% CF/PTFE/graphite may be an ideal polymer for seawater hydraulic applications [10-12]. Therefore, six kinds of corrosion-resistant alloys (AISI 316, AISI 630, QAI9-4, Ti6Al4V, chromium-plated Ti6Al4V (C-Ti6Al4V) and nitrided Ti6Al4V (N-Ti6Al4V)) were prepared, and their tribocorrosion behavior against 30 vol.% CF/PTFE/graphite-filled PEEK was comparatively investigated; the optimal material combinations of PEEK with corrosion-resistant alloys for seawater hydraulic valve applications were then chosen.

2. EXPERIMENTS

2.1 Test rig

Tribocorrosion experiments were performed in a rotational friction tester (UMT TriboLab, Bruker) in pin-on-disk mode (as shown in Figure 1). A two-dimensional force sensor (up to 200 N load) was used to obtain the sliding and frictional data of the tribopair. During the test, the upper specimen was static while the bottom specimen was rotated by a servo motor, and the servo motor speed was controlled by a controller. The friction of the tribopair was detected by a force sensor in the data acquisition system.

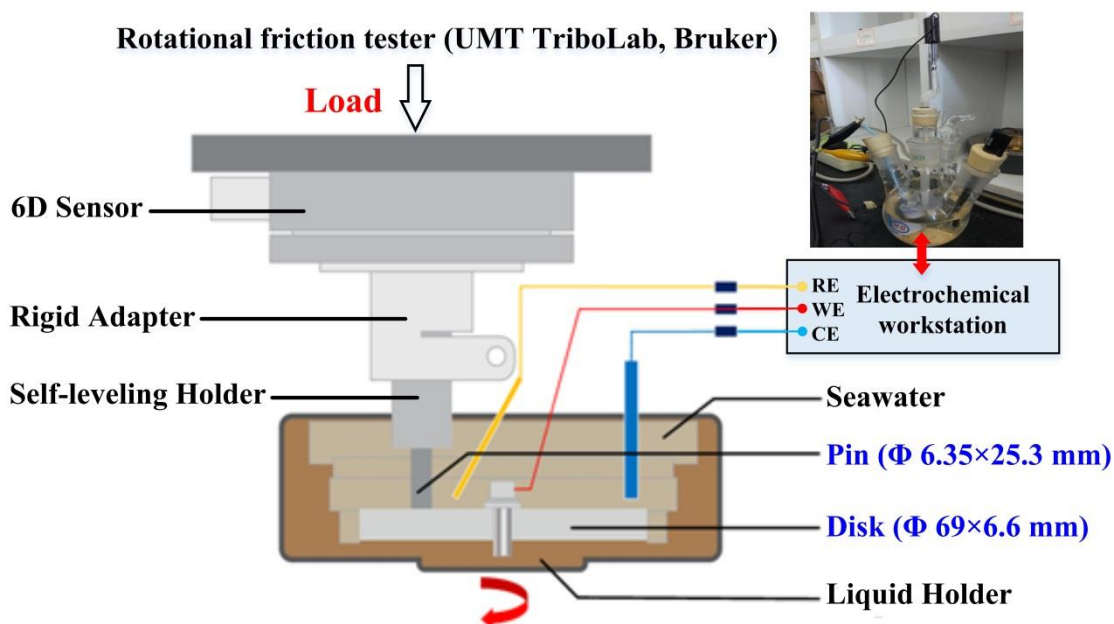


Figure 1. Schematic configuration of the pin-on-disk tribocorrosion test. RE: reference electrode, WE: working electrode, CE: counter electrode.

As illustrated in Figure 1, the electrochemical test module included three electrodes and was part of an improved tribological tribometer connected to a CS350 electrochemical workstation. During the test, the electrochemical workstation was employed to obtain the potentiodynamic polarization curves of corrosion-resistant alloys before and after tribological testing and to measure the open

potentials. The potentiodynamic and potentiostatic were measured by the platinum counter electrode and saturated calomel reference electrode (SCE). The electrical conductivity of the upper specimen (PEEK) could be neglected, and the liquid holder was made of polytetrafluoroethylene (PTFE).

2.2 Specimens and lubricants

The upper pin, with dimensions of $\Phi 6.35$ mm \times 25.3 mm, was made of CF-PEEK contained 30% volume fraction CF and formed through a hot-pressing, sintering and molding technology. The main mechanical characteristics of the CF-PEEK composite are shown in Table 1.

Table 1. Main mechanical characteristics of the CF-PEEK composite

Property	Standard	Unit	Value
Density	ISO 1183	g/cm ³	1.44
Water absorption (24 h, 23°C)	ISO 62	%	0.06
Rockwell hardness	ASTM D785	—	102
Tensile strength (23°C)	ASTM D638	MPa	134
Bending strength (23°C)	ASTM D790	MPa	186
Compressive strength (23°C)	ASTM D695	MPa	150
Coefficient of thermal expansion	ASTM D696	10 ⁻⁵ /°C	2.2

Table 2. Main physical performance of AISI 630, AISI 316, QA19-4, Ti6Al4V, C-Ti6Al4V and N-Ti6Al4V

Materials	Density (g/cm ³)	Tensile strength (MPa)	Yield strength (MPa)	Hardness (HV)
AISI 630	7.78	1070	1000	386
AISI 316	7.98	620	310	351
QA19-4	7.50	540	300	180
Ti6Al4V	4.40	915	830	395
C-Ti6Al4V	—	—	—	876
N-Ti6Al4V	—	—	—	1180

The lower disks, with dimensions of $\Phi 69$ mm \times 6.6 mm, were made of AISI 316, AISI 630, QA19-4, Ti6Al4V, C-Ti6Al4V and N-Ti6Al4V. The major physical performance parameters of these corrosion-resistant alloys are listed in Table 2. The contact surface roughness R_a of the specimens, prepared by grinding and diamond antiscuffing paste polishing, was approximately 0.1 μ m. A TK-5C surface profiler was used to measure the contact surface roughness of the specimens. In addition, the

specimens were submerged in tap water for seven days before the test to avoid the effect of hygroscopicity on dimensional and weight during the experiment.

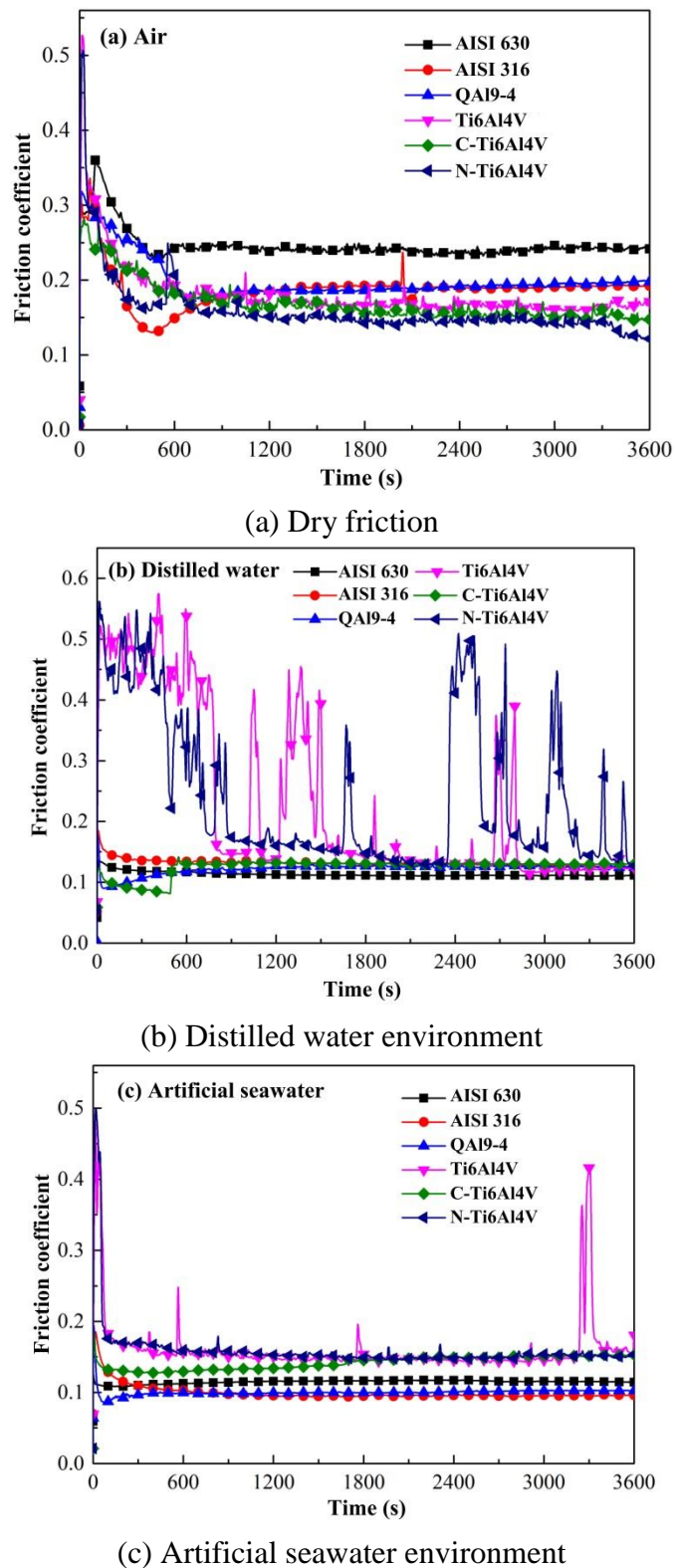
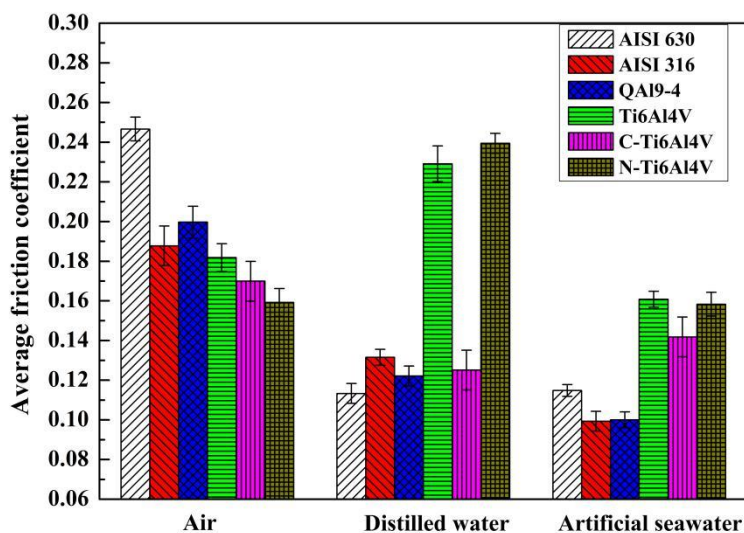


Figure 2. Friction coefficients of several corrosion-resistant alloys sliding against CF-PEEK: (a) in air, (b) in distilled water and (c) in artificial seawater.

Table 3. Main chemical elements of artificial seawater

Element	Concentration (g/l)	Element	Concentration (g/l)
Na ⁺	9.92	Cl ⁻	18.01
Mg ²⁺	1.16	SO ₄ ²⁻	2.25
Ca ²⁺	0.38	CO ₃ ²⁻	0.025
K ⁺	0.36	HCO ₃ ⁻	0.075

Note: Salinity is 3.2%, pH value is 8.2

**Figure 3.** Steady-state average friction coefficients of different alloys sliding against CF-PEEK.

In this study, the seawater was composed of tap water and artificial tropical marine crystal sea salt, according to the GB 17378.4-2007 standard. Before preparation, a large quantity of tap water was placed in the sun for seven days to allow sufficient chlorine volatilization, and the artificial sea salt was fully dissolved in the thus obtained tap water. The salinity and pH value of the artificial seawater were approximately 8.2 and 3.2%, respectively. The content of each element in the prepared seawater was very close to that in natural seawater, and the contents of the main chemical elements in the artificial seawater are shown in Table 3.

2.3 Test methods

To study the tribocorrosion characteristics of several corrosion-resistant alloys sliding against CF-PEEK, a series of experiments were carried out: (1) Sliding wear experiments were carried out with the rotation speed of 200 r/min, load of 200 N, mean rotation radius of 20 mm, environmental temperature of approximately 20 °C, and duration of 3600 s. (2) Potentiodynamic tests, which involve obtaining the polarization curves of the tribopair under static corrosion, were started after reaching a stable open circuit potential (OCP). (3) Tribocorrosion experiments were conducted under OCP conditions, and the change process of OCP was measured. During the static corrosion and

tribocorrosion tests, the potential varies from -200 mV to +400 mV with a sweep rate of 0.3 mV/s. The measurements were repeated three times for each testing condition.

The total weight loss including contributions from abrasion, corrosion and the interaction between these two, is defined by

$$W_t = W_{corr} + W_{wear} + \Delta W \quad (1)$$

$$\Delta W = \Delta W_c + \Delta W_w \quad (2)$$

where W_t is the total tribocorrosion weight loss, W_{corr} is the pure corrosion weight loss, W_{wear} is the pure abrasion weight loss, ΔW is the synergetic weight loss between mechanical wear and corrosion, ΔW_c is the wear-induced corrosion and ΔW_w is the corrosion-induced wear.

In addition, the total abrasion-corrosion weight loss W_t can be expressed as

$$W_t = W'_{corr} + W'_{wear} \quad (3)$$

where W'_{corr} and W'_{wear} are the corrosion weight loss and abrasion weight loss under tribocorrosion conditions, respectively.

With Eq. (1) to (3), the W'_{corr} and W'_{wear} can be obtained as follows:

$$W'_{corr} = W_{corr} + \Delta W_c \quad (4)$$

$$W'_{wear} = W_{wear} + \Delta W_w \quad (5)$$

Before and after the test, all the specimens were cleaned ultrasonically with anhydrous alcohol, dried with hot air, and then weighed by an electronic balance (Ohaus CP214) with discretion of 0.1 mg to obtain the weight loss Δm . The wear rate W_s can be obtained as

$$W_s = \frac{\Delta m}{\rho F_N L} \quad (\text{mm}^3/\text{Nm}) \quad (6)$$

where ρ is the specimen density, F_N represents the normal load, and L is the total sliding distance. The mean friction coefficients were measured by the online data acquisition system throughout the whole test process.

W_t and W_{wear} were measured by the Ohaus CP214 electronic balance during the friction and wear tests, respectively, conducted in seawater and distilled water. W_{corr} and W'_{corr} were measured under static corrosion and corrosive wear, respectively, by the CS350 electrochemical workstation. Then, W'_{wear} , ΔW_w , ΔW_c and ΔW were calculated by Eqs. (1) to (5). The corrosion weight loss W_m was calculated by Faraday's law based on the electrochemical test data [20]:

$$W_m = \frac{Itm}{nF} \quad (7)$$

where I is the current in amperes, t is the time in seconds, n is the electron valence of the metal, F is Faraday's constant, and m is the metal atomic mass.

To investigate the tribological mechanism, the worn surface micrographs of the specimens were observed by 3D microscopy with the aid of a superwide depth of field microscope (VHX-5000).

3. RESULTS AND DISCUSSION

3.1 Friction and wear performance

The friction coefficients of several corrosion-resistant alloys sliding against the CF-PEEK composite in different environments are shown in Figure 2. As illustrated in Figure 2(a), when sliding in air, the friction coefficients of all the tribopairs initially increased, then gradually decreased and stabilized after the running-in process. A similar phenomenon has previously been reported [10]. As presented in Figure 2(b), the CF-PEEK/Ti6Al4V and CF-PEEK/N-Ti6Al4V tribopairs did not operate steadily when sliding in distilled water. Nevertheless, the friction coefficients of AISI 630, AISI 316, QA19-4 and C-Ti6Al4V rapidly stabilized after a short running-in process. Figure 2(c) shows that the friction coefficients of all the corrosion-resistant alloys decreased when sliding in artificial seawater.

As shown in Figure 3, the average friction coefficients of the alloys in water lubrication are lower than those under dry friction conditions. This difference is because the adsorbed water molecules improved the lubrication effect of the tribopair. This result was consistent with the current literature [16, 17]. In addition, the average friction coefficients of the same alloys lubricated with distilled water are higher than those when lubricated with artificial seawater. This difference is because the active element Cl in seawater reacted with the alloys and then produced an easy-shear tribolayer on the lower disks [21]. Moreover, the ferric oxide, ferric sulfide and ferric chloride in the easy-shear tribolayer improved the lubrication performance of the tribopair. Thus, the average friction coefficients of the tribopairs decreased under artificial seawater lubrication. These results and analyses are consistent with Shan's research [18].

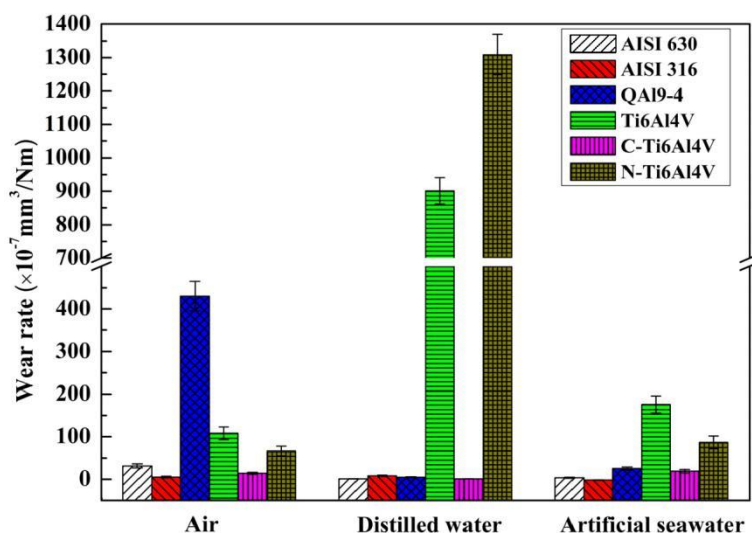


Figure 4. The wear rates of different alloys when sliding on CF-PEEK.

The wear rates of different alloys when sliding on CF-PEEK under different lubrication conditions are presented in Figure 4. Figure 4 illustrates that the wear rate of AISI 316 is minimal in air and seawater. This minimal wear rate occurred because of the good corrosion resistance of AISI 316, which is consistent with the experimental results obtained by Obadele [22]. In particular, the lowest value was $1.01 \times 10^{-7} \text{ mm}^3/\text{N}\cdot\text{m}$ for AISI 630 in distilled water. In addition, the wear rates of

Ti6Al4V and N-Ti6Al4V were quite large with distilled water lubrication and were much higher than those with dry sliding and seawater lubrication. However, the wear rate of C-Ti6Al4V was low, which was attributed to the increase in Ti6Al4V surface hardness caused by the chromium plating process. Consequently, AISI 630, AISI 316 and C-Ti6Al4V presented better tribological characteristics when sliding in air, distilled water and artificial seawater conditions.

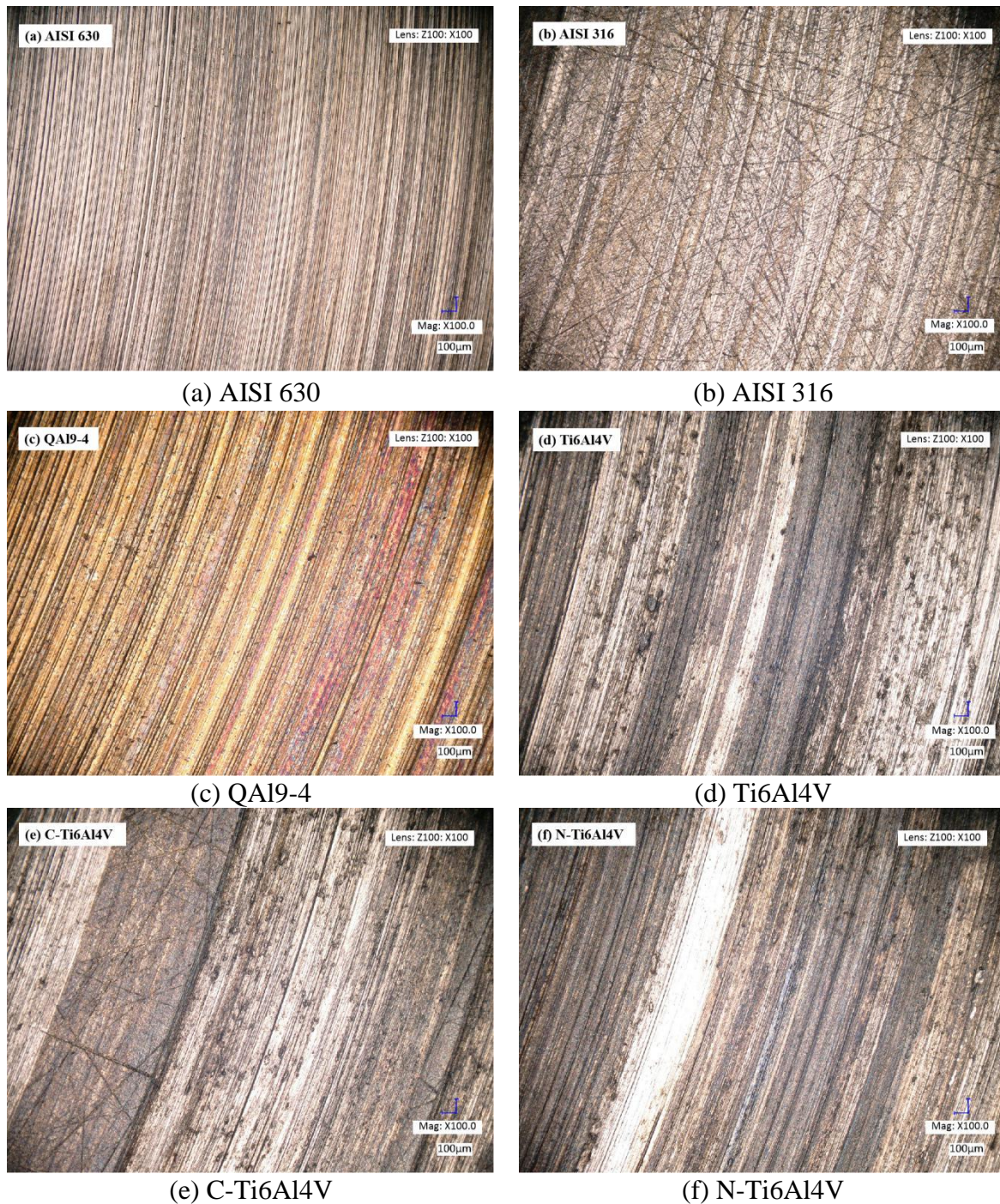


Figure 5. Optical micrographs of different alloys under tribocorrosion conditions in artificial seawater: (a) AISI 630, (b) AISI 316, (c) QA19-4, (d) Ti6Al4V, (e) C-Ti6Al4V and (f) N-Ti6Al4V.

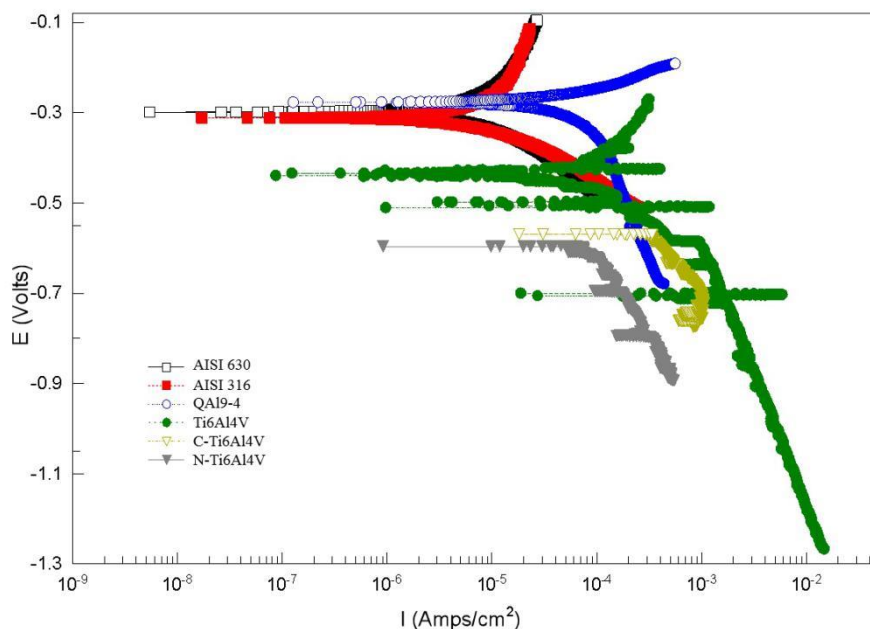


Figure 6. Polarization curves of different alloys in artificial seawater under static corrosion.

Figure 5 illustrates the worn surfaces of different alloys sliding against CF-PEEK under tribocorrosion conditions. As shown in Figures 5(a) and 5(b), the wear tracks of AISI 630 and AISI 316 were shallow and flat. Figure 5(c) reveals the existence of obvious corrosion on the surface of QAI9-4. It is evident from Figures 5(d) to 5(f) that the wear tracks on Ti6Al4V, C-Ti6Al4V and N-Ti6Al4V were coarse and wide. In addition, some grooves and delamination are displayed in Figures 5(d) to 5(f). The wear observed in these images occurred because the inadequate mechanical characteristics of the Ti6Al4V alloy make tribochemical and mechanical wear the dominant wear mechanisms [18]. Thus, the wear rates and friction coefficient of Ti6Al4V, C-Ti6Al4V and N-Ti6Al4V were higher than those of AISI 630 and AISI 316.

3.2 Static corrosion behavior

The static corrosion test was conducted to study corrosion behavior without any mechanical wear influence. To investigate the static corrosion behavior of the specimens, anodic polarization curves were measured under the sweep rate of 0.3 mV/s in artificial seawater. Scanning began after 20 min of immersion, starting at 200 mV below the corrosion potential and ending at a current density of at least $10 \mu\text{A}/\text{cm}^2$ [13]. Figure 6 and Table 4 show the obtained polarization curves under static corrosion. AISI 630, AISI 316 and QAI9-4 presented similar behavior, with close polarization potentials and polarization currents. The polarization potentials of Ti6Al4V and C-Ti6Al4V were relatively low, and N-Ti6Al4V clearly had the lowest polarization potential. In addition, it is clear from Figure 6 that the trend in polarization potential for the three kinds of Ti6Al4V, from high to low, was $\text{Ti6Al4V} > \text{C-Ti6Al4V} > \text{N-Ti6Al4V}$. More importantly, no passive regions of C-Ti6Al4V or N-Ti6Al4V were observed in Figure 6. Therefore, the seawater corrosion resistance of C-Ti6Al4V and N-Ti6Al4V was less than that of the original Ti6Al4V.

Table 4. Electrochemical parameters for different alloys under static conditions in seawater

Material	E_{corr} (V)	E_{b10} (V)	I_p ($\mu\text{A}/\text{cm}^2$)
AISI 630	-0.299	-0.244	0.747
AISI 316	-0.311	-0.260	0.108
QA19-4	-0.277	-0.272	2.565
Ti6Al4V	-0.184	-0.430	0.024
C-Ti6Al4V	-0.488	—	5.398
N-Ti6Al4V	-0.247	-0.596	0.179

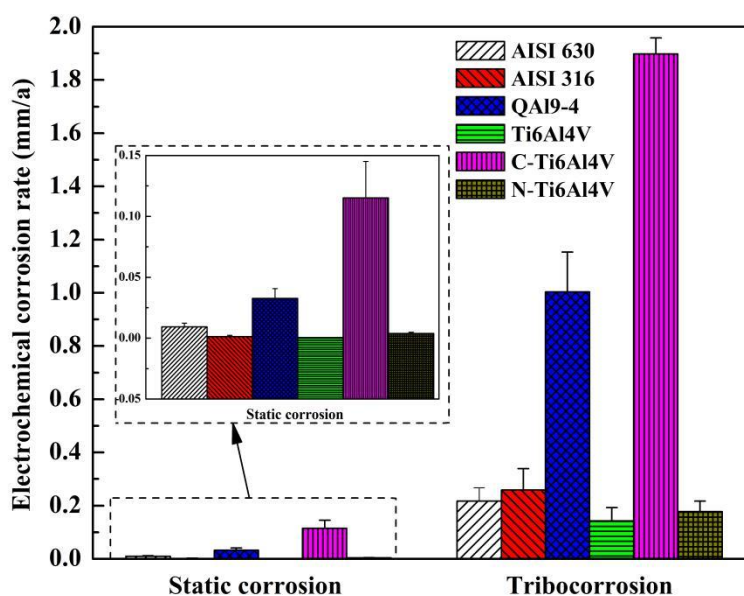


Figure 7. Electrochemical corrosion rate of different alloys under static corrosion and tribocorrosion conditions in seawater.

3.3 Wear-corrosion synergy

Tribocorrosion tests of different alloys in artificial seawater were conducted. Figure 7 shows the corrosion rates of different alloys under static corrosion and tribocorrosion conditions lubricated with seawater. Ti6Al4V showed the lowest corrosion rate under both static corrosion and tribocorrosion conditions. In addition, the maximum observed corrosion rate was that of C-Ti6Al4V and was approximately four orders of magnitude higher than that of the original Ti6Al4V. This trend is due to the passive oxide film on the C-Ti6Al4V surface being removed or damaged. Therefore, it can be concluded that the chromium plating process did not improve the corrosion-resistance of Ti6Al4V.

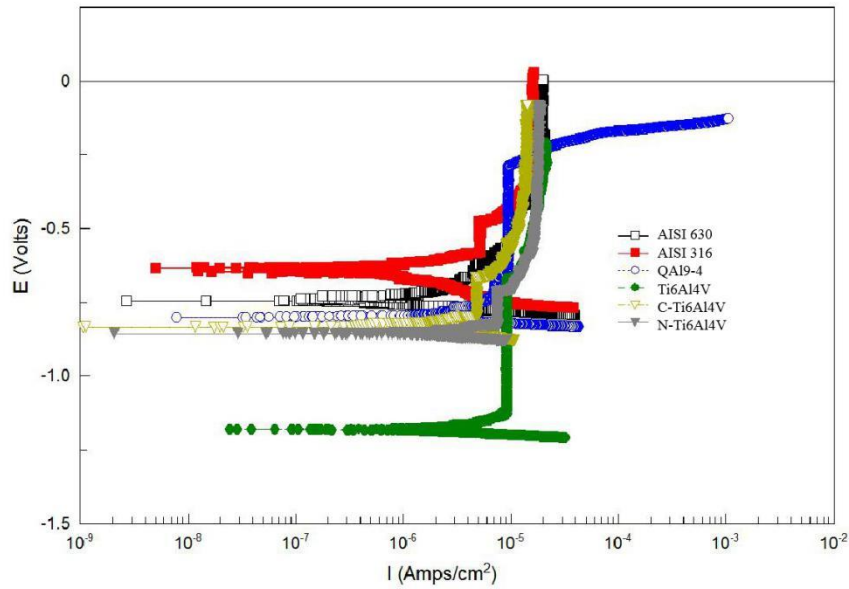


Figure 8. Polarization curves of the six studied kinds of alloys in artificial seawater under tribocorrosion.

Figure 8 shows the Tafel polarization curves of the six kinds of alloys, and Table 5 lists the corrosion potential E_{corr} , the pitting potential E_{b10} and the corrosion current density I_p . Figure 8 shows that the corrosion potentials of the alloys were all negative and the corrosion rate increased with increasing corrosion current density [23]. Moreover, AISI 316 resulted in the highest corrosion potential of -0.6 V.

Table 5. Electrochemical parameters for different alloys under tribocorrosion conditions in seawater

Material	E_{corr} (V)	E_{b10} (V)	I_p ($\mu\text{A}/\text{cm}^2$)
AISI 630	-0.746	-0.458	17.372
AISI 316	-0.634	-0.422	21.527
QAl9-4	-0.801	-0.286	78.865
Ti6Al4V	-1.182	-0.670	6.615
C-Ti6Al4V	-0.834	-0.565	88.950
N-Ti6Al4V	-0.857	-0.707	8.147

The lowest corrosion potential (-1.1815 V) was observed during the corrosion testing of Ti6Al4V. As shown in Table 5, the I_p of Ti6Al4V was lower than those of the other alloys, and the I_p of C-Ti6Al4V was much higher than those of N-Ti6Al4V and the original Ti6Al4V. The trend in I_p for the six kinds of alloys, from high to low, was C-Ti6Al4V > QAl9-4 > AISI 316 > AISI 630 > N-Ti6Al4V > Ti6Al4V. Therefore, Ti6Al4V exhibited the maximum corrosion resistance among the six kinds of alloys.

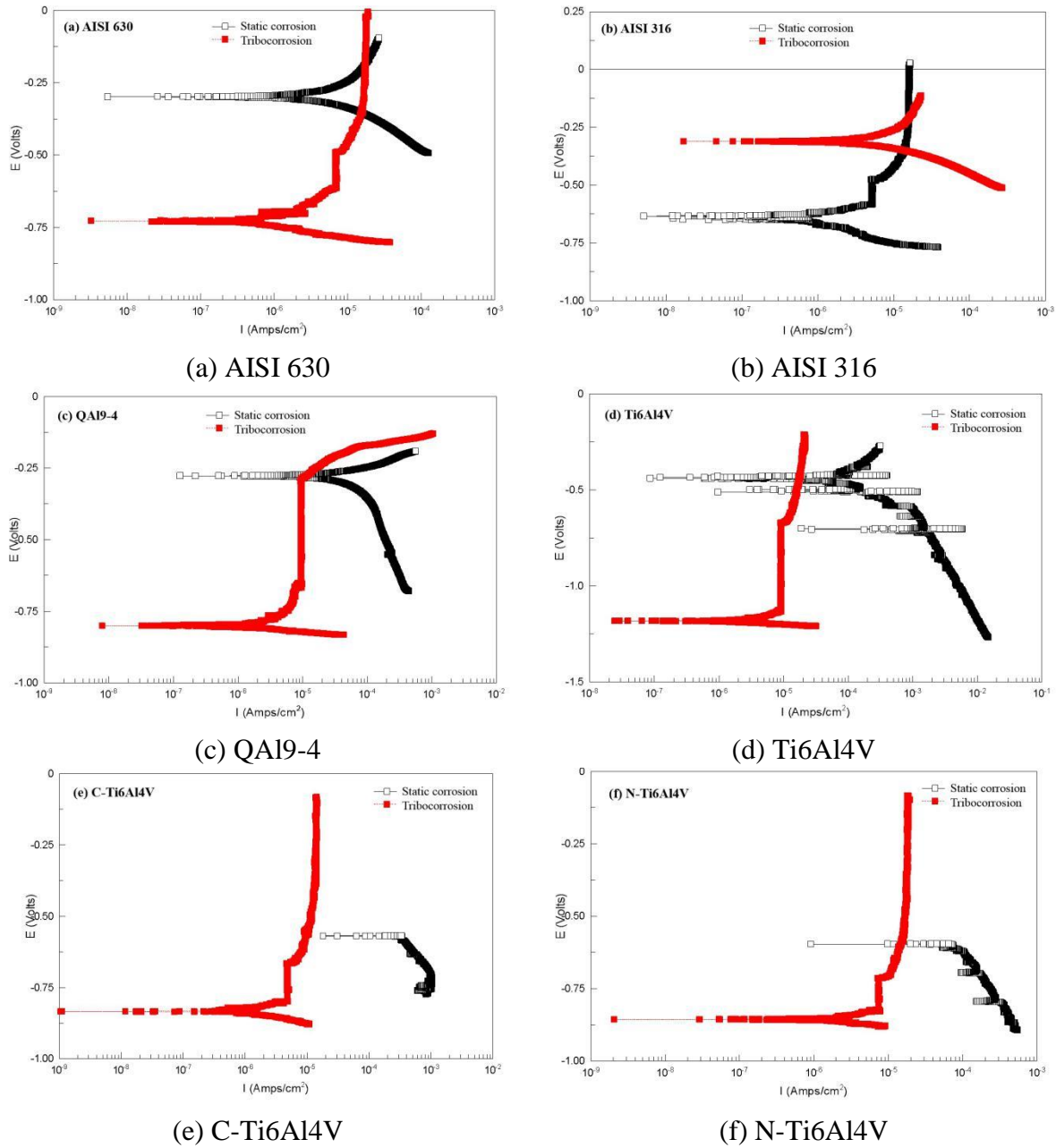


Figure 9. Polarization curves of different alloys under static corrosion and tribocorrosion conditions in seawater: (a) AISI 630 (b) AISI 316 (c) QAI9-4 (d) Ti6Al4V (e) C-Ti6Al4V and (f) N-Ti6Al4V.

Based on the sliding wear, static corrosion and tribocorrosion tests, the proportions of mechanical wear and corrosion in material loss under lubrication with artificial seawater were also studied. As shown in Table 6, ΔW_c is obviously smaller than ΔW_w for all alloys. The contribution of corrosion-induced wear to synergetic weight loss was more than 85% for all the alloys. This value is attributed to the difficulty of formation of passive oxide films in artificial seawater [24]. In addition, as CF-PEEK slides on the alloy surface, sliding wear and corrosion-induced wear increase the material loss in the tribocorrosion process. Therefore, the passive oxide film formed on the original alloy surface is easily destroyed, which is the main cause of material loss. This behavior agrees with other

works [19, 23-26]. Moreover, the ratio of $\Delta W_c/\Delta W$ is negligibly small for Ti6Al4V and N-Ti6Al4V. The ratio of $\Delta W_c/\Delta W$ for C-Ti6Al4V is approximately 14%, which indicates that the corrosion resistance of C-Ti6Al4V is relatively poor under tribocorrosion conditions in seawater.

Table 6. Contribution of synergistic effect for different alloys in seawater

Material loss	Corrosion-resistant alloys					
	AISI 630	AISI 316	QA19-4	Ti6Al4V	C-Ti6Al4V	N-Ti6Al4V
ΔW (mm/a)	1.923	-6.826	14.5349	-508.360	12.616	-857.182
ΔW_w (mm/a)	1.711	-7.083	13.563	-508.218	10.834	-857.008
ΔW_c (mm/a)	0.207	0.2572	0.971	-0.1423	1.783	-0.173
$\Delta W_w/\Delta W$ (%)	89.198	103.768	93.320	99.972	85.870	99.980
$\Delta W_c/\Delta W$ (%)	10.802	-3.768	6.680	0.0280	14.130	0.020

Figure 9 and Table 7 show the polarization curves of alloys sliding against CF-PEEK under static corrosion and tribocorrosion conditions. Figure 9 shows that the tribocorrosion potential is more negative than the pure corrosion potential for all the alloys, which indicates that mechanical sliding could reduce the alloy corrosion potential and increase the corrosion tendency. The current densities of AISI 630 and AISI 316 had almost the same magnitude. An obvious passive region can be seen in Figures 9(b) and 9(d), which indicates that AISI 316 and Ti6Al4V are very negative and have strong corrosion resistance when immersed in seawater [26]. In addition, when E_{corr} was higher than 0.5 V, secondary passivity of AISI 316 was observed (Figure 9(b)), and the current density in the secondary passive region increased. This secondary passivity occurred because the passive oxide film on AISI 316 was restructured at high potential [27].

Table 7. Electrochemical parameters of different alloys under static and tribocorrosion conditions in seawater. S: static, T: tribocorrosion.

Parameters	AISI 630		AISI 316		QA19-4		Ti6Al4V		C-Ti6Al4V		N-Ti6Al4V	
	S	T	S	T	S	T	S	T	S	T	S	T
E_{corr} (V)	-0.30	-0.75	-0.31	-0.63	-0.28	-0.80	-0.18	-1.18	-0.49	-0.83	-0.25	-0.86
E_{b10} (V)	-0.24	-0.46	-0.26	-0.42	-0.28	-0.29	-0.43	-0.67	—	-0.57	-0.60	-0.71
I_p ($\mu\text{A}/\text{cm}^2$)	0.75	17.37	0.11	21.53	2.565	78.87	0.02	6.615	5.40	88.95	0.18	8.15

4. CONCLUSIONS

The tribological and corrosive behavior of several corrosion-resistant alloys (AISI 316, AISI 630, QA19-4, Ti6Al4V, C-Ti6Al4V and N-Ti6Al4V) sliding against CF-PEEK were investigated in artificial seawater. Based on the above results, the following important conclusions can be obtained:

1. The friction coefficient of most alloys in distilled water and artificial seawater is lower than that in a dry friction environment. The rank of steady-state average friction coefficients was Ti6Al4V > N-Ti6Al4V > C-Ti6Al4V > AISI 630 > QA19-4 > AISI 316. The tribological properties of Ti6Al4V and N-Ti6Al4V are the worst. However, AISI 630, AISI 316 and C-Ti6Al4V exhibit better tribological behavior under dry friction, distilled water and artificial seawater conditions.

2. Wear-corrosion synergy is obvious in alloys sliding against CF-PEEK under tribocorrosion conditions lubricated with artificial seawater, and the corrosion-induced wear is higher than the wear-induced corrosion. The contribution of corrosion-induced wear to synergetic weight loss is more than 85% for all the alloys.

3. The corrosion resistance of Ti6Al4V is higher under static corrosion and tribocorrosion conditions. However, the corrosion resistance of C-Ti6Al4V is poor under both static corrosion and tribocorrosion conditions. The chromium plating process accelerated the Ti6Al4V corrosion rate in seawater, which is not suitable for seawater hydraulic valves. Therefore, the material combinations of AISI 630/CF-PEEK and AISI 316/CF-PEEK could preferentially be used in seawater hydraulic valves.

ACKNOWLEDGEMENTS

The authors would like to thank the Beijing Natural Science Foundation (Nos 3182003 and 1184012), National Natural Science Foundation of China (Nos 51705008 and 11572012), China Postdoctoral Science Foundation funded project (No 2017M620551), Beijing Municipal Science and Technology Project (No KM201810005014 and KM201910005033), Beijing Postdoctoral Research Foundation (No 2017-ZZ020) and CSIC Key Laboratory of Thermal Power Technology Open Foundation (No TPL2017BB010) for their funding for this research. The authors are very grateful to the editors and the anonymous reviewers for their insightful comments and suggestions.

References

1. H. Y. Yang, M. Pan, *J. Zhejiang Univ.-Sc. A.*, 16 (2015) 427.
2. L. S. Drabløs, *Desalination* 183 (2005) 41.
3. F. L. Yin, S. L. Nie, H. Ji, Y. Q. Huang, *Ocean Eng.*, 163 (2018) 337.
4. X. Y. Liu, S. L. Nie, G. H. Li, F. L. Yin, *J. Braz. Soc. Mech. Sci. A.*, 40 (2018) 11.
5. J. K. Lancaster, *Tribol. Int.*, 23 (1990) 371.
6. F. Majdic, J. Pezdernik, M. Kalin, *Tribol. Int.*, 44 (2011) 2013.
7. D. F. Wu, Y. S. Liu, D. L. Li, X. F. Zhao, C. Li, *Ocean Eng.*, 131 (2017) 107.
8. J. Z. Wang, F. Y. Yan, Q. J. Xue, *Wear*, 267 (2009) 1634.
9. B. B. Chen, J. Z. Wang, F. Y. Yan, *Tribol. Int.*, 52 (2012) 170.
10. Z. Q. Wang, D. R. Gao, *Mater. Des.*, 51 (2013) 983.
11. W. T. Dong, S. L. Nie, A. Q. Zhang, *Proc. Inst. Mech. Eng. J. J. Eng. Tribol.*, 227 (2013) 1129.
12. Z. H. Zhang, S. L. Nie, S. H. Yuan, W. J. Liao, *Tribol. T.*, 58 (2015) 1096.
13. A. López, R. Bayón, F. Pagano, A. Igartua, A. Arredondo, J. L. Arana, J. J. González, *Wear*, 338 (2015) 1.
14. J. Chen, F. Y. Yan, *Trans. Nonferrous Met. Soc. China*, 22 (2012) 1356.
15. J. Chen, Q. Zhang, Q. A. Li, S. L. Fu, J. Z. Wang, *Trans. Nonferrous Met. Soc. China*, 24 (2014) 1022.
16. J. Chen, J. Z. Wang, F. Y. Yan, Q. Zhang, Q. A. Li, *Tribol. Int.*, 81 (2015) 1.

17. Y. Zhang, X. Y. Yin, F. Y. Yan, *Mater. Chem. Phys.*, 179 (2016) 273.
18. L. Shan, Y. X. Wang, Y. R. Zhang, Q. Zhang, Q. J. Xue, *Wear*, 362-363 (2016) 97.
19. F. Zhou, Q. Ma, Q. Z. Wang, Z. F. Zhou, L. K. Y. Li, *Tribol. Int.*, 116 (2017) 19.
20. P. Ponthiaux, F. Wenger, D. Drees, J. P. Celis, *Wear*, 256 (2004) 459.
21. L. Shan, Y. X. Wang, J. L. Li, H. Li, X. D. Wu, J. M. Chen, *Surf. Coat. Technol.*, 226 (2013) 40.
22. B. A. Obadele, M. L. Lepule, A. Andrews, P. A. Olubambi, *Tribol. Int.*, 78 (2014) 160.
23. J. Chen, J. Z. Wang, B. B. Chen, F. Y. Yan, *Tribol. T.*, 54 (2011) 514.
24. B. A. Obadele, A. Andrews, M. B. Shongwe, P. A. Olubambi, *Mater. Chem. Phys.*, 171 (2016) 239.
25. Y. K. Xu, H. M. Qi, G. T. Li, X. P. Guo, Y. Wan, G. Zhang, *J. Colloid Interf. Sci.*, 518 (2018) 263.
26. W. Aperador, A. Delgado, J. Bautista-Ruiz, *Int. J. Electrochem. Sci.*, 10 (2015) 9408.
27. J. Chen, F. Y. Yan, B. B. Chen, J. Z. Wang, *Mater. Corros.*, 64 (2013) 394.

© 2019 The Authors. Published by ESG (www.electrochemsci.org). This article is an open access article distributed under the terms and conditions of the Creative Commons Attribution license (<http://creativecommons.org/licenses/by/4.0/>).